Available online at www.sciencedirect.com

ScienceDirect

Biomedical Journal

journal homepage: www.elsevier.com/locate/bj

Original Article

Effect of despeckling filters on the segmentation of ultrasound common carotid artery images

Vaishali Narendra Naik [a,*], *R.S. Gamad* [b], *P.P. Bansod* [b]

[a] *Department of Electronics and Communication Engineering, Shri Govindram Sakseria Institute of Technology and Science, Indore, Madhya Pradesh, India*

[b] *Department of Electronics and Instrumentation Engineering, Shri Govindram Sakseria Institute of Technology and Science, Indore, Madhya Pradesh, India*

ARTICLE INFO

Article history:
Received 10 September 2016
Accepted 7 July 2021
Available online 15 July 2021

Keywords:
Atherosclerosis
Carotid artery
Intima-media thickness
Segmentation
Despeckle filter

ABSTRACT

Background: Carotid intima-media thickness (IMT) measured in B-mode ultrasound image is an important indicator of Atherosclerosis disease. Speckle noise inherently present in ultrasounds' thereby degrades the visual evaluation and limits the automated segmentation performance. The objective of this study is to investigate the effects of three despeckle filters on the segmentation of carotid IMT in ultrasound image.

Methods: Automated segmentation of IMT is achieved by utilizing fast fuzzy c-mean clustering and distance-regularized level set without re-initialization techniques. Manual segmentation has been done by an experienced radiologist. The performances of median, hybrid median and improved adaptive complex diffusion (IACDF) filters are examined and a quantitative and qualitative comparison among these filters has been reported on 151 DICOM images. Bland–Altman plots were used to compare IMT results of these filters.

Furthermore, performances of above three filters are evaluated under different noise levels by individually adding speckle and salt and pepper noise in ten randomly selected images from 151 DICOM dataset. Plots between noise and quality evaluation metric parameters are used to compare de-noising performance of these filters.

Results: The average processing time per image of proposed IMT measurement technique without-filter and with filter is approx 15.39 s max.

Conclusion: It is shown that the median filter (window 5 × 5) measures better than hybrid median and IACDF filters. Finally, concluded that de-noising of ultrasound image before segmentation procedure certainly improves segmentation accuracy. Furthermore, it is observed that these filters do not impose serious computational burden and entail moderate processing time.

* *Corresponding author*. Department of Electronics and Communication Engineering, Shri Govindram Sakseria Institute of Technology and Science, 23 Park Rd., Indore 452003, Madhya Pradesh, India.

E-mail addresses: vai9naik@gmail.com (V.N. Naik), rsgamad@gmail.com (R.S. Gamad), ppbansod43@gmail.com (P.P. Bansod).

Peer review under responsibility of Chang Gung University.

https://doi.org/10.1016/j.bj.2021.07.002

At a glance of commentary

Scientific background on the subject

Carotid Intima-Media Thickness (IMT) is used to detect the atherosclerosis disease. Assessment of IMT via segmentation of B-mode ultrasound common carotid artery is cheap, reliable and safe for the patients. Speckle noise is inherently present in ultrasounds' which limits the automated segmentation performance. It should be reduced through despeckle filters.

What this study adds to the field

In this study, despeckle filters, i.e., (i) Median, (ii) Hybrid median and (iii) Improved adaptive complex diffusion are examined and a quantitative and qualitative comparison among these filters has been reported. The experimental results show that filtering certainly improves segmentation accuracy without imposing a serious computational burden and entail moderate processing time.

Cardiovascular disease is a major cause of increasing death rate which is commonly caused by atherosclerosis. Intima-Media Thickness (IMT) is used to detect the atherosclerosis disease and is defined as the distance between lumen - intima (LI) and media -adventitia (MA) interfaces. Assessment of IMT via segmentation of B-mode ultrasound CCA is cheap, reliable and safe for the patients. Although ultrasound manifests the benefit of being real time, the B-mode images are prone to speckle noise and have a low signal to noise ratio, which degrades the visual evaluation and limits the automated segmentation performance [1–3]. For optimum segmentation performance, it should be reduced without affecting the important information of the images. The simplest way to reduce speckle noise is by median filter with a proper window size. Numerous despeckle techniques exist in the literature which are based on local statistics [4], Wiener [5], median [6], geometric [7], wavelet, total variational filter, anisotropic diffusion [8], empirical mode decomposition (EMD) [9,10], frequency & spatial compounding [11]. In Ref. [12] Argenti, Fabrizio et al. presented a comprehensive review of despeckling techniques; in this study, authors have discussed speckle noise reduction techniques in synthetic aperture radar images. In Ref. [13] Loizou Christos P. et al. demonstrated several despeckle filtering methods. The authors reported that the mean and variance local statistics filter (lsmv) performance was the best, subsequently the Geometric despeckle filter (gf4d) and the local-statistics minimum speckle-index homogeneous mask filter (lsminsc). The majority of speckle reduction techniques have drawbacks such as: sensitivity to size and shape of the window, dependence on threshold value and inhibiting smoothing near the edges. In Ref. [14] Al-Karawi et al., proposed an adaptive block-based trainable approach by using support vector machine classifier to detect regions and target the speckle noise of the detected regions instead of the whole image.

The performance of de-speckle filter can be evaluated by utilizing texture analysis, visual evaluation by the experts and image quality metrics such as mean absolute, mean square error (MSE), root mean square, geometric average errors and error summation in the form of the Minkowski metric, signal -to- noise ratio (SNR), peak signal-to-noise ratio (PSNR), universal quality index (Q), structural similarity index (SSIM), metric based on natural scene statistics and mutual information between the original and the filtered images [15].

Recently, in Ref. [16] Biswas, Mainak, et al. presented a review of artificial intelligence-based methods such as Machine learning and deep learning used in the detection and measurement of IMT. These techniques are used for monitoring CVD/stroke risk. In 2021 [17] Abd-Ellah et al. demonstrated a regional convolutional neural network based method to detect CCA disease.

The objective of this study is to evaluate the effect of despeckle filters on the CCA segmentation performance. Here, segmentation is achieved by combining standard clustering technique and distance regularized level set without re-initialization scheme (DRLSE) [18]. Clustered image obtained from fast-fuzzy c-mean clustering (FFCM) [19] is used to create desirable mask which is used as a region of interest (ROI) in final segmentation (here DRLSE) scheme. Polyline distance metric (PDM) is used to measure IMT distance [20,21]. In this work, filtering performance of median [6], hybrid median [22] and IACDF [23] despeckling filters have been evaluated. This paper is organized as follows: second section presents methodology; third section presents the experimental results and discussion followed by conclusion.

Materials and methods

Dataset and specification of processing machine

In this work, 151 longitudinal B-mode ultrasound CCA images of DICOM format are utilized which were acquired by the LOGIQ-P5 GE healthcare ultrasound equipment with a resolution of 614 × 816 pixels with 256 gray levels. The images have been randomly selected from normal and asymptomatic subjects that were under comprehensive routine clinical screening. Some images have soft plaques. MATLAB 7.14.0.739 (R2012a) on machine having widescreen 16:9 (aspect ratio) 15.6″ display at 1366 × 768 resolution, Intel (R) Core (TM) i5-2430M processor at speed 2.40 GHz with 4 GB RAM is used to segment the boundaries of distal (far wall) IMT layer.

Proposed IMT measurement scheme

The block diagram of IMT measurement scheme is shown in [Fig. 1] [24]. The proposed procedure consists of five steps, i.e. pre-processing, clustering, final segmentation of IMT followed by measuring thickness of detected IMT and lastly statistical analysis. The steps are briefly described as follows:

Pre-processing

Pre-processing generally includes cropping and filtering operations and ROI selection. The algorithm was developed to crop B-mode ultrasound CCA image automatically (to

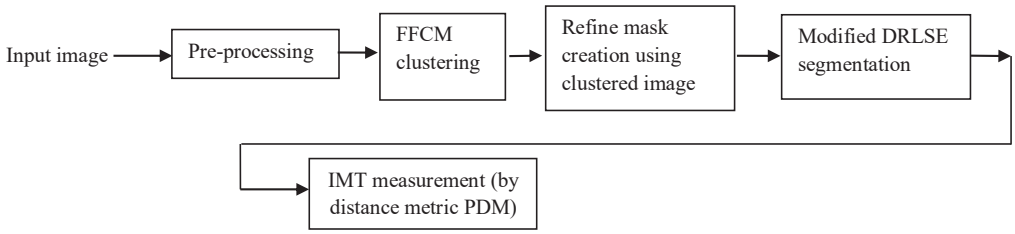

Fig. 1 Block diagram of IMT measurement scheme.

enhance clustering performance) and after filtering ROI is manually selected by user. Filtering is necessary as in ultrasound, speckle noise exists inherently and degrades the quality of an image and limits the segmentation performance. This multiplicative speckle noise in ultrasound may be approximated as additive white Gaussian noise if the envelope signal is captured after logarithmic compression. Therefore to improve segmentation accuracy it should be filtered out without affecting the important features of the images. Here three different Despeckle filters are individually applied to reduce speckle noise and their performance is also evaluated by adding speckle noise and salt and pepper noise independently to 10 samples (randomly selected from dataset).

Median filter. The median filter computes the median value in a local neighborhood of each pixel [6]. The median filter performance is sensitive to size of the window and therefore is evaluated using window size 3 × 3 ($MedianW_3$), 5 × 5 ($MedianW_5$) and 7 × 7 ($MedianW_7$) and experimental results reveal that $MedianW_5$ has the best performance.

Hybrid median filter. The hybrid median filter [22] also called as corner preserving median filter is a three-step ranking operation. In N x N pixel neighborhood, pixels are ranked in two different groups. The median values of the 45° and 90° neighbors' forming an "x" and "+" respectively, are compared with the central pixel and the median value of the set, is then saved as the new pixel value. In this study, hybrid median performance of window size 3 × 3 ($H\_medianW_3$), 5 × 5 ($H\_medianW_5$) and 7 × 7 ($H\_medianW_7$) is evaluated and was observed that $H\_medianW_7$ is better than $H\_medianW_3$ and $H\_medianW_5$.

IACDF. The generalized equation for nonlinear anisotropic complex diffusion filter is given [23] by,

$$\frac{\partial I}{\partial t} = div(D\nabla I) \tag{1}$$

where, ∇ is the gradient, I is image and D is the diffusion coefficient. Diffusion coefficient in terms of laplacian of I (ΔI) is expressed as:

$$D \approx 1/1 + (\Delta I/k)^2 \tag{2}$$

where k is a controlling parameter which controls the spreading of the diffusion coefficient in the vicinity of its maximum i.e. at edges and homogeneous areas, where ΔI vanishes. If k = constant for the entire image and for iteration (2) preserving the location of edges. In order to preserve the location of edges as well as the variation of intensity across the edge k is defined as:

$$k = k_{max}(k_{min} - k_{max})\frac{g - min(g)}{max(g) - min(g)} \tag{3}$$

and

$$g = \nabla G_{N,\sigma} * Re(I) \tag{4}$$

where * is the convolution operator, $\nabla G_{N,\sigma}$ is local average (gaussian) kernel of size N x N and σ is standard deviation. Parameters values kept are: $\theta = \frac{pi}{30}$, $N = 3$, $k_{min} = 2$, $k_{max} = 28$ *and* $\sigma = 10$ same as in Ref. [23].

Conventionally, in nonlinear complex diffusion processes time step (Δt) is a constant. The adaptive time step is selected; a small step size is used at the initial iterations in which higher values of D can be found due to the speckle noise. At steady conditions in which changes over time are small (fraction-wise), the time step selected is larger, while at fast changes in time the time step selected is smaller.

$$\Delta t^{(n)} = \frac{1}{\alpha}\left[a + bexp\left\{-max\left(\left|Re\left(\partial I/\partial t\right)\right| \Big/ Re(I^{(n)})\right)\right\}\right] \tag{5}$$

where constant α is 4 for 2D images, parameters a *and* b control the time step with $a + b \leq 1$. The advantage of this formulation is that the k parameter values need not to be defined beforehand; instead, it adapts itself to the data. The main controlling parameter of the IACDF is diffusion time (t_D) in sec; its performance is evaluated for 0.5, 0.55, 0.6, 0.65, 0.7, 0.75, 0.8, 0.85, 0.9, 0.95, 1, 2 and 3 and was observed that optimum performance was obtained at 0.75 s.

Fast fuzzy c-mean clustering scheme

Fuzzy c-mean is an unsupervised clustering technique in which a data point belongs to all classes with different degree of membership. Clustering is achieved by iteratively minimizing the objective function. It divides n data points into c fuzzy clusters. Firstly, initialized centroids of the cluster's memberships for all the data points are calculated based on the relative (Euclidian) distance of the data points from the centroids of the clusters followed by updating them along with membership function. The membership function signifies the probability that a pixel belongs to a specific cluster. The process converges to a solution when the updated centroids represent the local minimum of the objective function. After convergence, each data points are assigned to a specific cluster for which the membership is maximal [25]. To improve

the processing time, clustering is performed on the histogram of the image intensities instead of the raw image data [19]. Concretely, the objective function (J_F) used for Fast Fuzzy c-mean is defined as:

$$J_F = \sum_{i=1}^{c} \sum_{g=0}^{q-1} \gamma_g u_{ig}^m ||g - v_i||^2 \quad (6)$$

where, g is gray level of the image, v_i represents centre of the i^{th} cluster, c is the number of clusters, u_{ig} is the fuzzy membership of gray value g with respect to cluster i, λ_g is the number of pixels having gray value equal to g, where $g = 0, .., q-1$ here, q is the number of gray levels and is generally much smaller than total no. of pixels (N):

$$N = \sum_{g=0}^{q-1} \gamma_g \quad (7)$$

The centroids (v) are initialized as $v = (g_{min} + dg/2 : dg : g_{max})$, here g_{min} & g_{max} are minimum and maximum gray levels of the image, respectively and change in gray level is $dg = \left(\frac{g_{max} - g_{min}}{c}\right)$.

The membership functions and cluster centres are as follows:

$$u_{ig} = 1 \Big/ \sum_{i-1}^{c} \left(\frac{||g_g - v_i||}{||g_g - v_c||}\right)^{2/(m-1)} \quad (8)$$

and

$$v_i = \sum_{k=0}^{q-1} u_{ik}^m h(k) k \Big/ \sum_{k=0}^{q-1} u_{ik}^m h(k) \quad (9)$$

The first and last clusters represent the average intensity of lumen and adventitia respectively in image [19]. From the large number of experiments it is observed that optimum clustering is obtained by selecting number of $c = 6$.

Final IMT segmentation scheme

Standard DRLSE scheme is modified and utilized as final segmentation method to detect LI and MA interfaces in CCA image. A brief description of the scheme is given as follows:

Level set is a numerical technique for capturing moving fronts, basic evolution equation of level set function (LSF) $\varphi(t, x, y)$ is:

$$\frac{\partial \varphi}{\partial t} + \mathcal{F}|\nabla \varphi| = 0 \quad (10)$$

where $\mathcal{F}$ is the speed parameter, which depends on image data & LSF. The distance regularized level set without re-initialization the LSF evolution equation is given [18]:

$$\frac{d\varphi}{dt} = \mu div\left(d_p(|\nabla \varphi|)\nabla \varphi\right) + \lambda\, \delta_\varepsilon(\varphi)\, div\left(g \frac{\nabla \varphi}{|\nabla \varphi|}\right) + \alpha\, g\, \delta_\varepsilon(\varphi) \quad (11)$$

and

$$d_p \triangleq p(s)'/s \quad (12)$$

where $\mu > 0$ is constant, λ coefficient of weighted length term, δ_ε is dirac function, α coefficient of weighted area term, $p(s)$ is potential function and g edge indicator is defined in the terms of Gaussian kernel G_σ with standard deviation (σ)

$$g = \frac{1}{1 + |\nabla G_\sigma * I|^2} \quad (13)$$

In the modified DRLSE scheme, g in equation (13) is redefined to incorporate the effect of fuzzy boundaries of an image, modified edge indicator function is:

$$g_2 = g + \vartheta g_1 \quad (14)$$

and

$$g_1 = \frac{1}{1 + |\nabla G_\sigma * I_1|^2} \quad (15)$$

where I_1 clustered image and parameter is ϑ controls the amount of fuzziness incorporated with the DRLSE edge indicator function. Here ϑ is computed automatically from image I. Finally, the modified DRLSE evolution equation is given as:

$$\frac{d\varphi}{dt} = \mu div\left(d_p(|\nabla \varphi|)\nabla \varphi\right) + \lambda\, \delta_\varepsilon(\varphi)\, div\left(g_2 \frac{\nabla \varphi}{|\nabla \varphi|}\right) + \alpha\, g_2\, \delta_\varepsilon(\varphi) \quad (16)$$

In this work, to achieve optimization the parameter's values selected as per the previous study [26] are: $\lambda = 5$, $\alpha = 10.5$, $\varepsilon = 1.5$, $\mu = 0.04$, $\sigma = 1.5$, $C_o = 3$. The number of iteration (N_t) is computed automatically by utilizing intensity information within the ROI.

Distance measurement between LI and MA interfaces by PDM

The distance between the detected LI and MA interfaces are measured by PDM as it is a clinically suitable distance measurement technique for computing IMT [20,21]. The measured IMT is in pixels (in image coordinate system) and requires pixel to metric unit conversion. It is possible to calibrate an image as the ruler is embedded in it, for 151 dataset calibration factor obtained is within 0.0312–0.1206 mm and effective length of the pixel is equal to calibration factor of an image. Thereby, IMT measurement error comprises of calibration error.

Statistical analysis procedure and quality evaluation metrics

Statistical analysis procedure. IMT measurement performance under different filters is assessed by computing parameters such as mean (μ), standard deviation (σ), coefficient of variation CV% (here, CV% $= (\sigma \times 100/\sqrt{2})/\mu$), correlation. In addition, Bland Altman plots are utilized to evaluate the effect of despeckles filters.

Quality evaluation metrics. To compare the performances of the filters, PSNR, Universal quality factor and Structural similarity index are measured which are defined as follows [17]:

(a) Peak Signal to Noise Ratio (PSNR): The PSNR is defined as:

$$PSNR = -10 \log_{10} MSE/g_{max}^2 \quad (17)$$

where g_{max} is maximum gray level in original image.

(b) *Universal quality index:* The quality index Q models distortions owing to loss of correlation, luminance distortion & contrast distortion is given as:

Table 1 Comparison between Manual, Without_F and Median filter (with square window size (N) = 3, 5 and 7) here measurand is IMT in mm.

n = 151	Manual	Without_F	MedianW$_3$	MedianW$_5$	MedianW$_7$
Mean	0.9536	1.004427	0.9832	0.9471	0.9063
std	0.2854	0.306744	0.2946	0.2824	0.2805
CV%	21.1597	21.59448	21.1849	21.0860	21.8854
r	1	0.924617	0.9322	0.9823	0.9624
t_p (sec)	–	14.07	14.43	13.71	13.72

Abbreviations: n: number of samples; std: standard deviation; CV%: coefficient of variation; r: Pearson's correlation; t_p: average processing time.

$$Q = \frac{\sigma_{IF}}{\sigma_F \sigma_I} \cdot \frac{2\bar{F}\bar{I}}{\left(\bar{F}\right)^2 + \left(\bar{I}\right)^2} \cdot \frac{2\sigma_F \sigma_I}{\sigma_F^2 + \sigma_I^2} \quad -1 < Q < 1 \tag{18}$$

where $\bar{I}$ and $\bar{F}$ represents the mean of the original and filtered values with their standard deviations and covariance, σ_I, σ_F and σ_{IF} respectively. To compute Q, a sliding window of size 8×8 without overlapping is used.

(c) *Structural similarity index*: The SSIM between the two images is given by:

$$SSIM = \frac{\left(2\bar{I}\bar{F} + C_1\right)(2\sigma_{IF} + C_2)}{\left(\bar{I}^2 + \bar{F}^2 + C_1\right)(\sigma_F^2 + \sigma_I^2 + C_2)} \quad -1 < SSIM < 1 \tag{19}$$

where $C_1 = 0.01\, g_{max}$ and $C_2 = 0.03\, g_{max}$. *SSIM* is computed similar to the Q.

Experimental results and discussion

In this section, experimental results of three different filters (applied single time on an image) i.e. median, hybrid median and IACDF are comparatively presented. For automated IMT segmentation, proposed method is applied on 151 ultrasound B-mode images and the results are summarized in Tables 1–4 also presented Bland Altman plot shown in [Fig. S5 (A - H)].

Refer Table 1, mean (in mm) and standard deviation (CV %) for manual and automated IMT segmentation without filter (Without_F) are 0.9536 ± 0.2854 (21.1597%) and 1.0044 ± 0.3067 (21.5945%) respectively. Here, manual segmentation value is considered as ground truth (GT). The automated IMT mean and standard deviation (CV %) with MedianW$_3$, MedianW$_5$ and MedianW$_7$ are 0.9832 ± 0.2946 (21.1849%), 0.9471 ± 0.2824 (21.0860%) and 0.9063 ± 0.2805 (21.8854%) respectively. The correlation between manual and automated IMT Without_F is 0.924617; with MedianW$_3$, MedianW$_5$ and MedianW$_7$ are 0.9322, 0.9823 and 0.9624 respectively. [Fig. S5(A–C,H)] illustrate a Bland-Altman plot, the difference between the manual and the automated IMT measurements method is computed by mean ± 1.96SD (here SD is standard deviation). The mean ± 1.96SD for *Median*W$_3$, *Median*W$_5$, *Median*W$_7$ and Without_F are 0.03 ± 0.21, -0.01 ± 0.11, -0.05 ± 0.15 and 0.05 ± 0.23, respectively. From Table 1 and Fig. S5(A–C,H), it is observed that the performance of MedianW$_5$ is better than that Without_F, MedianW$_3$ and MedianW$_7$ thus for further comparison purpose MedianW$_5$ will be used. Due to speckle noise Without_F performance is poor. Under segmentation results in case of MedianW$_3$ as it fails to remove noise sufficiently (its performance certainly get improve if applied more than one time). Over segmentation results in case of MedianW$_7$, due to large window size edges get blurred.

The automated IMT mean (in mm) and standard deviation (CV %) with H_medianW$_3$, H_medianW$_5$ and H_medianW$_7$ are 0.9903 ± 0.3002 (21.4358%), 0.9715 ± 0.2953 (21.4891%) and 0.9469 ± 0.2914 (21.7588%) respectively. The correlation for H_medianW$_3$, H_medianW$_5$ and H_medianW$_7$ are 0.9350, 0.9416 and 0.9434 respectively [refer Table 2]. [Fig. S5(D–F,H)] illustrate a Bland–Altman plot, mean ± 1.96SD for *H_median*W$_3$, *H_median*W$_5$ and *H_median*W$_7$ are 0.04 ± 0.21, 0.02 ± 0.19 and −0.01 ± 0.19, respectively. Experimental results are summarized in [Table 2] and [Fig. S5(D–F,H)] reveals that performance of H_medianW$_7$ is better than Without_F, H_medianW$_3$ and H_medianW$_5$. Under segmentation results in case of H_medianW$_3$ and H_medianW$_5$ as it fails to remove noise sufficiently (its performance certainly get improve if applied more than one time).

Table 2 Comparison between Manual, Without_F and Hybrid median filter (with square window size 3, 5 and 7) here measurand is IMT in mm.

n = 151	Manual	Without_F	H_medianW$_3$	H_medianW$_5$	H_medianW$_7$
Mean	0.9536	1.0044	0.9903	0.9715	0.9469
std	0.2854	0.3067	0.3002	0.2953	0.2914
CV%	21.1597	21.5945	21.4358	21.4891	21.7588
r	1	0.9246	0.9350	0.9416	0.9434
t_p (sec)	–	14.07	14.04	14.34	14.28

Abbreviations: n: number of samples; std: standard deviation; CV%: coefficient of variation; r: Pearson's correlation; t_p: average processing time.

Table 3 Comparison between Manual, Without_F and IACDF filter (for t_D (sec): 0.5, 0.6, 0.65, 0.7, 0.75, 0.8, 0.85, 0.9 and 0.95) here measurand is IMT in mm.

n = 151	Manual	Without_F	$t_D = 0.5$	$t_D = 0.6$	$t_D = 0.65$	$t_D = 0.7$	$t_D = 0.75$	$t_D = 0.8$	$t_D = 0.85$	$t_D = 0.9$	$t_D = 0.95$	$t_D = 1$	$t_D = 2$	$t_D = 3$
Mean	0.9536	1.0044	0.9733	0.9720	0.9722	0.9684	0.9675	0.9621	0.9601	0.9479	0.9533	0.9542	0.9339	0.9198
std	0.2854	0.3067	0.2947	0.29459	0.2984	0.2989	0.2914	0.2948	0.2949	0.2916	0.2904	0.2934	0.2983	0.2994
CV%	21.1597	21.5945	21.4108	21.4228	21.7066	21.8238	21.2971	21.6646	21.7197	21.7518	21.5421	21.7391	22.5841	23.0156
r	1	0.9246	0.9615	0.9601	0.9600	0.9576	0.9617	0.9614	0.9587	0.8863	0.9601	0.9508	0.9462	0.9348
t_p (sec)	–	14.07	14.16	14.20	14.21	14.25	14.26	14.31	14.32	14.36	14.38	14.41	14.94	15.39

Abbreviations: n: number of samples; std: standard deviation; CV%: coefficient of variation; r: Pearson's correlation; t_p: average processing time; t_D: diffusion time.

The IMT mean (in mm), standard deviation, correlation and CV% for proposed method with IACDF filter for diffusion times (sec) 0.5, 0.6, 0.65, 0.7, 0.75, 0.8, 0.85, 0.9, 0.95, 1, 2 and 3 are computed and mentioned in [Table 3]. Table 3 illustrates optimum IMT performance obtained for diffusion time ranging from 0.5 s to 0.8 s. The highest correlation is obtained at diffusion time of 0.75 s. Thus for further comparison purpose the results at $t_D = 0.75$ s will be used. For IACDF at (t_D= 0.75 s) the IMT mean (in mm) and standard deviation (CV%, correlation) is 0.9675 ± 0.2914 (21.2971, 0.9617). [Fig. S5(G)] illustrates a Bland-Altman plot, the obtained mean ± 1.96SD (mm) for IACDF at (t_D= 0.75 s) is 0.01 ± 0.16. [Fig. S5(A–H)] depicts that IACDF is better than that of Without_F & hybrid-median but inferior to that of median filter.

The automated IMT measurements Without_F, MedianW_5, H_medianW_7 and IACDF ($t_D = 0.75$ s) filters are compared and summarized in [Table 4] and shown in [Fig. S5(A–H)]. From [Table 4] it is observed that automated IMT performance of Without_F is worst. The MedianW_5 is better than H_medianW_7 and IACDF ($t_D = 0.75$ s) filter. The average processing time per image of proposed IMT measurement technique Without_F and with filter is approx 15.39 s max (refer [Table 1-4]).

Fig. 2 illustrates the Box plot for the CCA IMT manual measurements and automated measurements (median filter window size 3 × 3, 5 × 5 and 7 × 7; hybrid median filter window size 3 × 3, 5 × 5 and 7 × 7; IACDF filter (at $t_D = 0.75$ s) and Without filter). Inter-Quartile Range (IQR), median, maximum, minimum and number of outliers values are shown above the box plots. No significant differences were found between the manual & the automated filtered IMT measurements methods, and significant difference was found between the manual & Without_F method (using the Wilcoxon rank-sum test): (i) Median filter (3 × 3): p = 0.2620, (ii) Median filter (5 × 5): p = 0.9916, (iii) Median filter (7 × 7): p = 0.1080, (iv) Hybrid median filter (3 × 3): p = 0.1466, (v) Hybrid median filter (5 × 5): p = 0.5447, (vi) Hybrid median filter (7 × 7): p = 0.8919, (vii) IACDF filter: p = 0.6031 and (viii) Without_F: p = 0.0354.

To evaluate the performance of the filters under different noise levels, they were tested for speckle and salt and pepper noise sources. The noises were added independently to the randomly selected 10 images from the 151 dataset. The MATLAB function $J = imnoise(I, 'type\ of\ noise', parameter)$ is used to add noise to the image I, here parameter variance (or density) value is 0, 0.05, 0.1, 0.15, 0.2 and 0.25. Performances of filters are evaluated by determining IMT on noise corrupted image and computing IMT accuracy, CV% and correlation for the noise level. Here accuracy is defined as difference between manual and automated value of IMT.

The IMT error for median, hybrid median and IACDF filter under noise levels 0–100% (0% represent variance or density = 0 and 100% represents variance or density = 0.25) are shown in [Figs. S6(A-C) and S7(A-C)] for speckle and salt and pepper noise respectively. In case of speckle noise, IMT error (in mm) for without filter, median, hybrid median and for IACDF filter is within −0.1814 to 0.0183, −0.0233 to 0.0270, −0.0698 to 0.0188 and −0.0171 to 0.0419 respectively. Similarly, in case of salt and pepper noise, IMT error for without filter, median, hybrid median and for IACDF filter is within 0.0183–0.4681, −0.0254 to 0.0178, −0.0042 to 0.0765 and −0.0053 to 0.1765 respectively.

Table 4 Comparison between Without_F, MedianW$_5$, H_medianW$_7$ and IACDF ($t_D = 0.75$) (measurand: IMT in mm).

n = 151	Manual	Without_F	MedianW$_5$	H_medianW$_7$	IACDF($t_D = 0.75$)
Mean	0.9536	1.004427	0.9471	0.9469	0.9675
std	0.2854	0.306744	0.2824	0.2914	0.2914
CV%	21.1597	21.59448	21.0860	21.7588	21.2971
r	–	0.924617	0.9823	0.9434	0.9617
t_p (sec)	–	14.07	13.71	14.28	14.26

Abbreviations: n: number of samples; std: standard deviation; CV%: coefficient of variation; r: Pearson's correlation; t_p: average processing time; t_D: diffusion time.

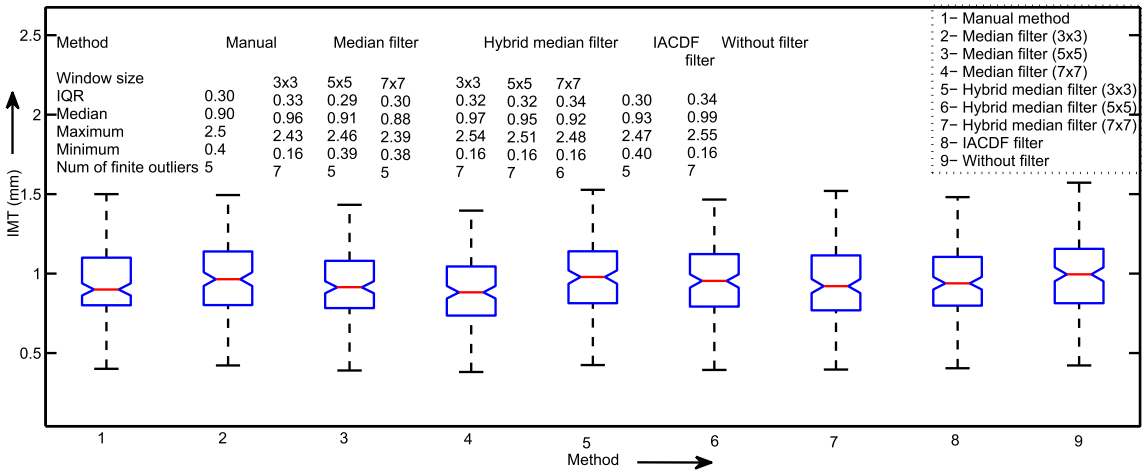

Fig. 2 Box plot for the CCA IMT manual measurements and automated measurements (median filter window size 3 × 3, 5 × 5 and 7 × 7; hybrid median filter window size 3 × 3, 5 × 5 and 7 × 7; IACDF filter (at $t_D = 0.75$ s) and Without filter). Inter-Quartile Range (IQR), median, maximum, minimum and number of outliers values are shown above the box plots.

Figs. S6(A-C) and S7(A-C) illustrates the addition of 0–100 percent noise segmentation of without-filtered image. This results in over-segmentation for speckle noise and mostly under-segmentation for salt and pepper noise. The segmentation accuracy fluctuates and mainly depends on the presence of noise on the LI and MA interfaces. In case of filtered image segmentation, accuracy depends upon filter's capability of removing noise and preserving edges. [Figs. S6(A-C) and S7(A-C)] depicts that segmentation accuracy with filter is superior to that of without-filter.

The coefficient of variation for manual segmentation method is 17.6763%. In case of speckle noise, CV% for proposed method without filter, median, hybrid median and for IACDF filter are within 17.2851%–36.4171%, 16.1734%–19.9380%, 17.5879%–26.2411% and 16.7187% to 21.1231% respectively. Similarly, in case of salt and pepper noise CV% for without filter, median, hybrid median and for IACDF filter are within 17.2296%–20.1786%, 16.7806%–18.4032%, 16.4992%–18.5406% and 14.6825%–20.1501% respectively. The plot between noise level and CV% for speckle and salt and pepper noise are presented in [Figs. S8(A-C) and S9(A-C)] respectively. In case of speckle noise, CV% for IACDF is better than without-filter, median and hybrid median filters, however for salt and pepper noise, CV% for median and hybrid median is comparable and is better than IACDF filter and without-filter.

The correlation between manual and automated methods is calculated and presented in [Figs. S10(A-C) and S11(A-C)]. In case of speckle noise, correlation for proposed method without-filter, median, hybrid median and for IACDF filter are within 0.4851–0.9934, 0.6461 to 0.9972, 0.6961 to 0.9961 and 0.7142 to 0.9931 (refer [Fig. S10(A-C)]). Similarly, in case of salt and pepper noise, correlation for without-filter, median hybrid median and for IACDF filter are within 0.5712–0.9934, 0.9804 to 0.9972, 0.9813 to 0.9961 and 0.7168 to 0.9911 (refer [Fig. S11(A-C)]). It is observed that segmentation performance of IACDF is superior to without-filter.

For a better comparison among median 5 × 5, hybrid median 7 × 7 and IACDF diffusion time 0.75, the IMT error, CV% and correlation plots against speckle and salt and pepper noise levels are presented in [Fig. 3(A-C) and 4(A-C)] respectively. It is observed that in case of speckle noise median 5 × 5, hybrid median 7 × 7 and IACDF (diffusion time = 0.75) filters performances are comparable (refer [Fig. 3(A-C)]). However, in case of salt and pepper noise, median 5 × 5, hybrid median 7 × 7 performances are better than IACDF (diffusion time = 0.75) filter (refer [Fig. 4(A-C)]).

Furthermore, filters performances are evaluated by computing average PSNR, average Universal quality index and average Structural Similarity index (SSIM) on 10 noise corrupted images. Noisy image is generated by adding noise to original image. Hence, original image is considered as noise free image. Therefore, average PSNR, average Universal quality index and average SSIM value of Without_F at noise level = 0 are considered as Ground truth value. Higher the

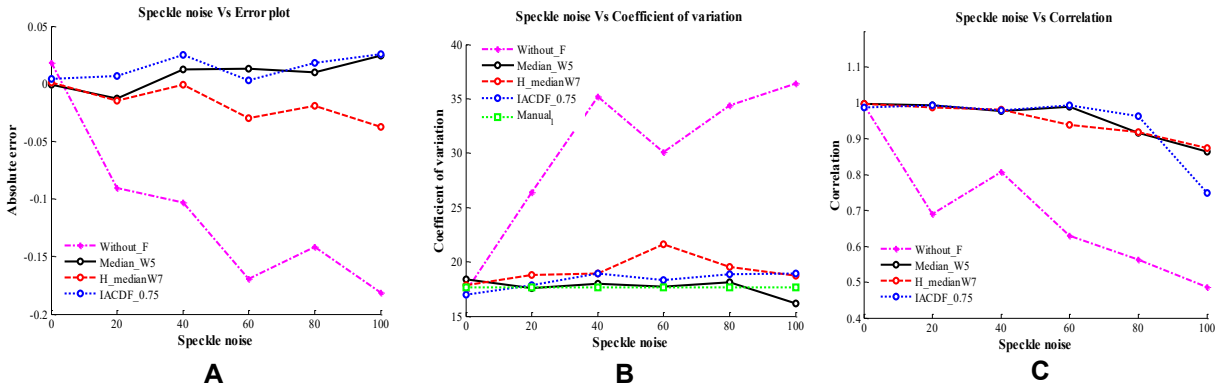

Fig. 3 Performance of Median_W5, H_medianW7 and IACDF_0.75 filters against speckle noise variance 0, 0.05, 0.1, 0.15, 0.2 and 0.25, plot between noise and (A) average IMT error; (B) average CV%; and (C) average correlation between manual and automated methods; calculated from a total of ten images.

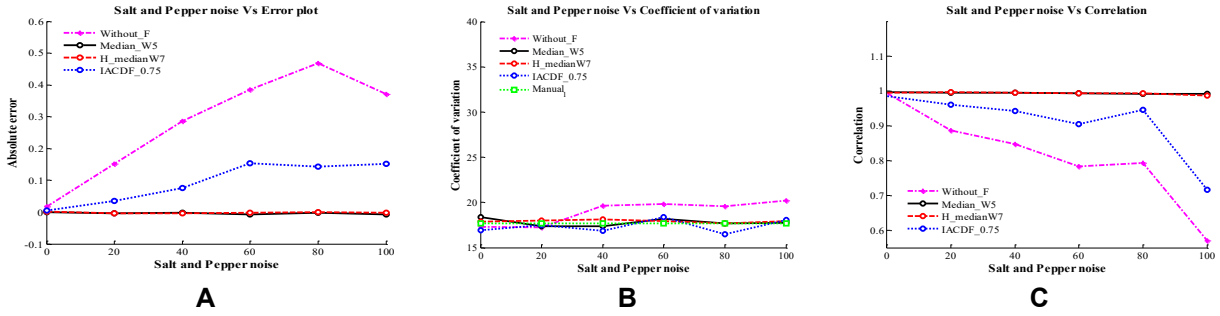

Fig. 4 Performance of Median_W5, H_medianW7 and IACDF_0.75 filters against salt and pepper noise density 0, 0.05, 0.1, 0.15, 0.2 and 0.25, plot between noise and (A) average IMT error; (B) average CV%; and (C) average correlation between manual and automated methods; calculated from a total of ten images.

value of PSNR, Universal quality index and SSIM better is the performance of the filter [13].

The plots between noise level and average PSNR for speckle noise and salt and pepper noise are presented (for median, hybrid median and IACDF filter) in [Figs. S12(A-C) and S13(A-C)]. The average PSNR value of Without_F at noise level = 0 is very high, for the sake of clarity it is not plotted in the graph. It is observed that for particular noise levels (except at 0% noise level) the obtained average PSNR value for with-filter (i.e., median, hybrid median and IACDF filter) is higher than that of average PSNR value for Without_F.

The plots between noise level and average Universal quality index for speckle noise and salt and pepper noise are presented (for median, hybrid median and IACDF filter) in [Figs. S14(A-C) and S15(A-C)] respectively. [Figs. S14(A-C) and S15(A-C)] depicts that Universal quality index for a particular noise level (except 0% noise level) obtained with-filter (i.e., median, hybrid median and IACDF filter) is higher than that of without-filter.

The plots between noise level and average SSIM index for speckle noise and salt and pepper noise are presented (for median, hybrid median and IACDF filter) in [Figs. S16(A-C) and S17(A-C)] respectively. [Figs. S16(A-C) and S17(A-C)] shows that mean SSIM index for a particular noise level (except 0% noise level) obtained with-filter is higher than that of without-filter.

For a better comparison among median 5 × 5, hybrid median 7 × 7 and IACDF (diffusion time 0.75), the average PSNR, average Universal quality index and average SSIM index plotted against speckle and salt and pepper noise levels are presented in [Figs. S18(A,B), S19(A,B) and S20(A,B)] respectively. While comparing without-filter, median 5 × 5, hybrid median 7 × 7 and IACDF diffusion time 0.75 average PSNR, average Q and average SSIM with-filter is higher than without-filter (above 0% noise level). In case of speckle noise, performances are analogous (refer [Fig. S18 (A)]); however, in case of salt and pepper noise, average PSNR of IACDF is lower than median 5 × 5 and hybrid median 7 × 7 (refer [Fig. S18 (B)]).

From [Figs. S19(A,B) and S20(A,B)], it is depicted that in case of speckle noise, performance of the filters are analogous to each other while for salt and pepper noise (for noise level above 0%) average Q and average SSIM of IACDF is lower than median 5 × 5 and hybrid median 7 × 7.

Conclusion

In this paper, a variational approach for CCA segmentation is developed by using two standard techniques, FFCM and DRLSE. The performance of the proposed segmentation method with median and hybrid median with window sizes

3 × 3, 5 × 5 & 7 × 7 and IACDF (for diffusion times 0.5, 0.6, 0.65, 0.7, 0.75, 0.8, 0.85, 0.9, 0.95, 1, 2 & 3 in sec) are evaluated by determining IMT in 151 samples. Moreover, its performance is evaluated by adding speckle and salt and pepper noise, independently, on10 randomly selected samples from 151 dataset. The segmentation accuracy in terms of average IMT error, mean, standard deviation, CV%, correlation, PSNR, Universal quality index and SSIM index parameters are used to evaluate the performance. The experimental results show that filtering certainly improves segmentation accuracy.

Optimum segmentation accuracy obtained for median with window size 5 × 5, hybrid median with window size 7 × 7 and IACDF with diffusion time 0.75. Performance of the median with window size 5 × 5 is slightly better than hybrid median and IACDF filters. In future, the performance of proposed segmentation technique (with-filter and without-filter) under Gaussian noise will be studied. Segmentation accuracy of proposed method using recently proved de-noising techniques such as TVF and EMD will be evaluated.

Funding

This research did not receive any specific grant from funding agencies in the public, commercial, or not-for-profit sectors.

Conflicts of interest

The authors have no financial or ethical conflicts of interest to report.

Acknowledgments

The authors express their gratitude to Dr. Chaitanya Puranik, HOD of Radio diagnosis and Dr. Deep Vora Radiologist, Vishesh hospital, Indore, for providing the data and help in manual segmentation.

Appendix A. Supplementary data

Supplementary data to this article can be found online at https://doi.org/10.1016/j.bj.2021.07.002.

REFERENCES

[1] Virani SS, Alonso A, Aparicio HJ, Benjamin EJ, Bittencourt MS, Callaway CW, et al. Heart disease and stroke statistics—2021 update: a report from the American Heart Association. Circulation 2021;143:254–743.
[2] Frostegård J. Immunity, atherosclerosis and cardiovascular disease. BMC Med 2013;11:117.
[3] Onut R, Balanescu AP, Constantinescu D, Calmac L, Marinescu M, Dorobantu PM. Imaging atherosclerosis by carotid intima-media thickness in vivo: how to, where and in whom? Maedica (Bucur) 2012;7:153–62.
[4] Lee JS. Refined filtering of image noise using local statistics. Comput Graph Imag Proc 1981;15:380–9.
[5] Baselice F, Ferraioli G, Johnsy AC, Pascazio V, Schirinzi G. Speckle reduction based on wiener filter in ultrasound images. Annu Int Conf IEEE Eng Med Biol Soc 2015;2015:3065–8.
[6] Huang TS, Yang GJ, Tang GY. A fast two-dimensional median filtering algorithm. IEEE Trans Acoust Speech Signal Proc 1979;27:13–8.
[7] Busse LJ, Crimmins TR, Fienup JR. A model based approach to improve the performance of the geometric filtering speckle reduction algorithm. In: 1995 IEEE Ultrasonics Symposium. Proceedings. An International Symposium 2, 2; 1995. p. 1353–6.
[8] Michailovich OV, Tannenbaum A. Despeckling of medical ultrasound images. IEEE Trans Ultrason Ferroelectr Freq Control 2006;53:64–78.
[9] Flandrin P, Rilling G, Goncalves P. Empirical mode decomposition as a filter bank. IEEE Signal Proc Lett 2004;11:112–4.
[10] Wu Z, Huang NE. Ensemble empirical mode decomposition: a noise-assisted data analysis method. Adv Adapt Data Anal 2009;1:1–41.
[11] Park J, Kang JB, Chang JH, Yoo Y. Speckle reduction techniques in medical ultrasound imaging. Biomed Eng Lett 2014;4:32–40.
[12] Argenti F, Lapini A, Bianchi T, Alparone L. A tutorial on speckle reduction in synthetic aperture radar images. IEEE Trans Geosci Rem Sens 2013;1:6–35.
[13] Loizou CP, Pattichis CS, Christodoulou CI, Istepanian RS, Pantziaris M, Nicolaides A. Comparative evaluation of despeckle filtering in ultrasound imaging of the carotid artery. IEEE Trans Ultrason Ferroelectr Freq Control 2005;52:1653–69.
[14] Al-Karawi D, Ibrahim D, Al-Assam H, Du H, Jassim S. A model-based adaptive method for speckle noise reduction in ultrasound images of ovarian tumours: a new approach. Multimodal Imag Exploit Learn 2021;11734:117340J.
[15] Loizou CP, Pattichis CS, Pantziaris M, Tyllis T, Nicolaides A. Quality evaluation of ultrasound imaging in the carotid artery based on normalization and speckle reduction filtering. Med Biol Eng Comput 2006;44:414–26.
[16] Biswas M, Saba L, Omerzu T, Johri AM, Khanna NN, Viskovic K, et al. A review on joint carotid intima-media thickness and plaque area measurement in ultrasound for cardiovascular/stroke risk monitoring: artificial intelligence framework. J Digit Imaging 2021;34:581–604.
[17] Abd-Ellah MK, Khalaf AAM, Gharieb RR, Hassanin DA. Automatic diagnosis of common carotid artery disease using different machine learning techniques. J Ambient Intell Human Comput 2021 May:236571206.
[18] Li C, Xu C, Gui C, Fox MD. Distance regularized level set evolution and its application to image segmentation. IEEE Trans Image Process 2010;19:3243–54.
[19] Anton Semechko. Fast fuzzy c-means image segmentation. GitHub, https://github.com/AntonSemechko/Fast-Fuzzy-C-Means-Segmentation/; 2021 [accessed 12 March 2014].
[20] Suri JS, Haralick RM, Sheehan FH. Greedy algorithm for error correction in automatically produced boundaries from low contrast ventriculograms. Pattern Anal Appl 2000;3:39–60.
[21] Saba L, Molinari F, Meiburger KM, Piga M, Zeng G, Rajendra Achraya U, et al. What is the correct distance measurement metric when measuring carotid ultrasound intima-media thickness automatically? Int Angiol 2012;31:483–9.

[22] Garcia Damien. Hybrid median filtering. MATLAB Central File Exchange. https://ww2.mathworks.cn/matlabcentral/fileexchange/25825-hybrid-median-filtering/; 2021 [accessed 10 May 2014].
[23] Bernardes R, Maduro C, Serranho P, Araujo A, Barbeiro S, Cunha-Vaz J. Improved adaptive complex diffusion despeckling filter. Opt Express 2010;18:24048–59.
[24] Naik VN, Gamad RS, Bansod P. Efficient initialisation of distance-regularised level set without re-initialisation scheme and quantitative evaluation of IMT in B mode ultrasound common carotid artery images. Comput Method Biomech Biomed Eng Imag Vis 2019;7:207–26.
[25] Bezdek JC, Ehrlich R, Full W. FCM: the fuzzy c-means clustering algorithm. Comput Geosci 1984;10:191–203.
[26] Naik V, Gamad RS, Bansod P. Implementation of three different segmentation techniques for quantitative evaluation of IMT in B-mode ultrasound common carotid artery images. Comput Method Biomech Biomed Eng Imag Vis 2016;4:317–26.